Parametric Analysis to Quantify Process Input Influence on the Printed Densities of Binder Jetted Alumina Ceramics

Edgar Mendoza Jimenez[1], Daming Ding[1], Laisuo Su[1], Aparna R. Joshi[2], Aarti Singh[2], B. Reeja-Jayan[1], Jack Beuth[1]

[1]Department of Mechanical Engineering, Carnegie Mellon University, Pittsburgh PA 15213
[2]Department of Machine Learning, Carnegie Mellon University, Pittsburgh PA 15213

ABSTRACT

Binder jetting, a commercial additive manufacturing process that selectively deposits a liquid binder onto a powder bed, can become a viable method to additively manufacture ceramics. However, the effects of process parameters/inputs on printing outputs (e.g. part density and geometric resolution) have not been investigated and no methodical approach exists for the process development of new materials. In this work, a parametric study consisting of 18 experiments with unique process input combinations explores the influence of seven process inputs on the relative densities of as-printed (green) alumina (Al_2O_3) parts. Sensitivity analyses compare the influence of each input on green densities. Multivariable linear and Gaussian process regressions provide models for predicting green densities as a function of binder jetting process inputs. The parametric study reveals that two process inputs, namely recoat speed and oscillator speed, significantly influence green densities. The multivariable linear and Gaussian process regression models indicate that the green densities of alumina builds can be increased by decreasing the recoat speed and increasing the oscillator speed. The Gaussian process regression model further suggests that the green densities have nonlinear dependence on the rest of the process parameters. Separate prints were performed at process input combinations different than those of the parametric study to validate the green density models. The models produced can assist operators in selecting process inputs that will result in a desired green density, allowing for the control of porosity in printed

parts with a high degree of accuracy. The methodology reported in this study can be leveraged for other powder systems and machines to predict and control the porosity of binder jetted parts for applications such as filters, bearings, electronics, and medical implants.

KEY WORDS: Binder Jetting, Ceramic, Alumina, Design of Experiments

1. INTRODUCTION

Rigorous developments in additive manufacturing (AM) processes, where materials are joined layer after layer to make objects from a 3D computer model, promote the introduction of novel manufacturing techniques and expansion of engineering design spaces [1]. The additive manufacturing of metals and plastics are currently being commercialized; metal and plastic builds are used in non-mission critical applications and undergoing certification for flight-critical components [2]. However, additive manufacturing of ceramic parts requires further development. Early work explored the AM of ceramics using stereolithography [3], direct energy deposition [4], powder bed fusion [5], and binder jetting processes [6]. Builds from these processes can be plagued with cracks or possess low relative densities compared to powder pressing techniques, and most of these processes require high-temperature (>1700 ℃) heat treatments to densify the printed parts [7].

Binder jetting, developed at the Massachusetts Institute of Technology in 1989 [8], can become a feasible solution to the AM of bulk ceramics. It is a commercial AM process that selectively deposits a liquid binder onto a powder bed. This process is compatible with most materials; metals (e.g. copper [9], stainless steel [10]), low purity alumina [6], barium titanite [11], and silicon nitride [12] are some of the materials that have demonstrated feasibility.

This study binder jets high purity (99%) alumina. With a projected demand of about $6.4 billion by 2020, alumina is the most widely used and studied technical ceramic as it accounts for 38% of all technical ceramics consumed by the United States [13]. Various industries utilize alumina because of its materials properties and low cost; applications include substrates and packages for electronics [14] [15], ballistic protection [16], filters [17], insulators for spark plugs [18], and medical implants [19]. Alumina is mostly used in the thermodynamically stable α phase, which has a hexagonally close-packed arrangement. α-Alumina has a density of 3.95 $\mathrm{g/cm^3}$ and hardness equal to 9 on the Mohs scale [20]. It possesses a melting temperature of 2050 ± 4 ℃ and thermal conductivity of about $20\ W/mK$, making it an effective thermal insulator [21]. It exhibits high abrasion and corrosion resistance over a large temperature range [22].

Low cost methods for manufacturing alumina include tape casting, dry pressing, and injection molding [16]. With that said, increasing the geometric complexity of alumina parts can drastically increase the cost of fabrication. Post-production machining constitutes as much as 75% of the cost in ceramic production [13]. An additive manufacturing process can produce near net-shaped parts of high geometric complexity, requiring little to no machining, and thus decrease ceramic fabrication costs.

Although binder jetting can become a viable method for fabricating geometrically complex ceramic parts without the need for post-production machining, there is no methodical approach for the process development of new materials. There is also little understanding of the relationship between process inputs and density of the printed parts [23]. Previous work explored the process optimization of binder jetting with metal powder systems, primitive machines, and focused on other process outputs (e.g. surface roughness, shrinkage during heat treatment) [6] [9] [10] [24] [25].

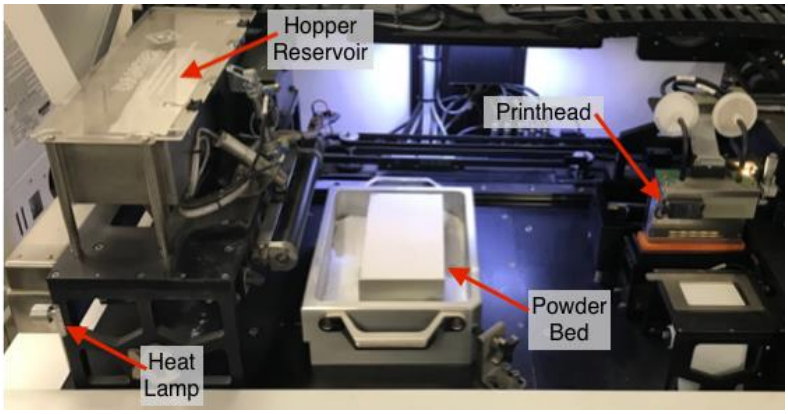

Figure 1. ExOne Innovent binder jetting system

Green densities, which are the densities of as-printed parts before any heat treatment postprocessing, significantly affect the quality and integrity of binder jetted parts. Part shrinkage is reduced and higher sintering densities are achieved with higher starting green densities [31] [32] [33]. Therefore, insights into controlling the green densities are necessary to binder jet high quality ceramics. Green and powder bed densities are dependent on particle size distribution, particle shape and the powder spreading system, but understanding the dependence of binder jetting process inputs is lacking [34] [35]. This research study uses an orthogonal design of experiments and sensitivity analyses to identify the process inputs that significantly influence printed green densities. A multivariable linear regression model is generated to predict green densities as a function of process inputs. A Gaussian process regression models is used to extrapolate parameters outside the studied process region that will maximize green densities. Findings can be leveraged to control the porosity of binder jetted parts for dielectric and other industrial applications.

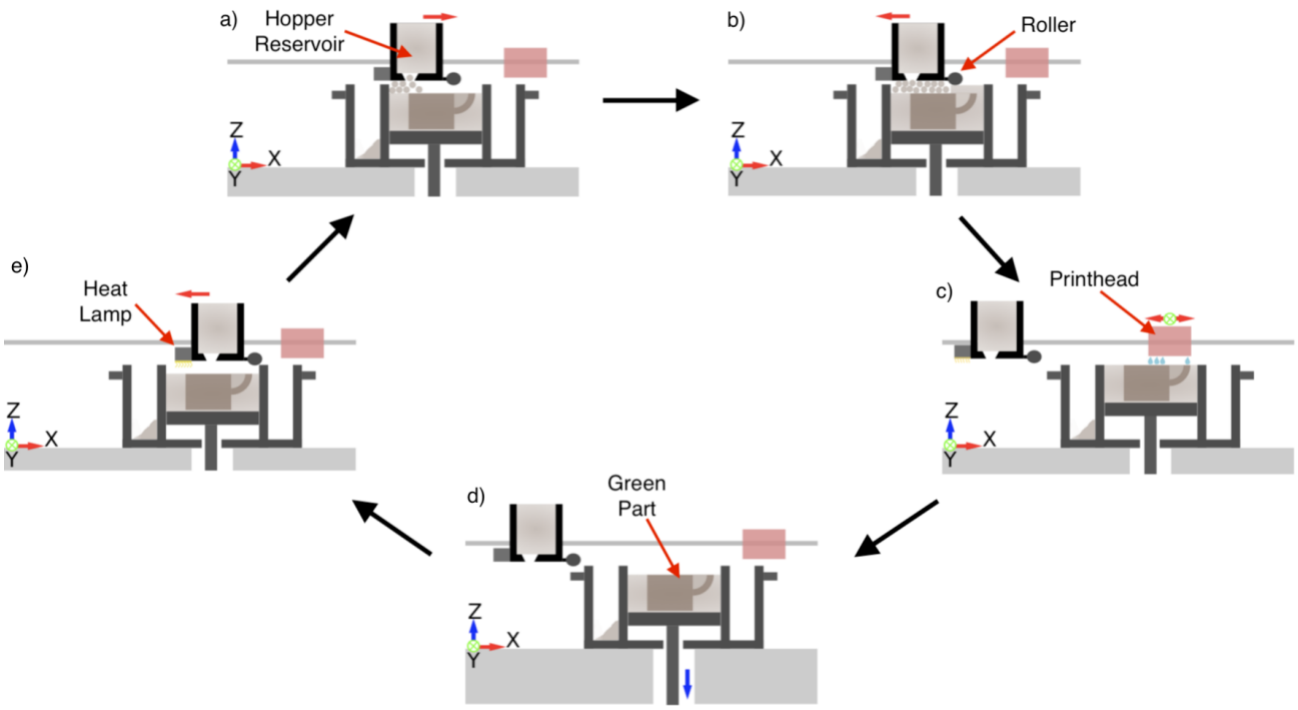

Figure 2. Printing process in binder jetting: (a) hopper reservoir oscillates to deposit powder onto the powder bed, (b) roller passes over newly deposited powder to create a flat layer, (c) printhead selectively deposits binder onto the top of the powder bed, (d) platform holding the powder bed lowers to allow for the deposition of a new layer of powder, and (e) heat lamp partially dries deposited binder before the next layer is deposited. The process repeats until the part is completed.

2. EXPERIMENTAL METHODS

2.1. Fabrication

Parts were fabricated via binder jetting using the Innovent Machine manufactured by ExOne (North Huntingdon, PA, USA), as seen in Figure 1. This particular machine possesses a build envelope of 65 x 65 x 160 mm and a printhead with 256 nozzles. The ExOne Innovent utilizes a hopper system where the powder is stored in a hopper bin to be later deposited. During the build process, the print head selectively deposits an aqueous binder onto a flat powder bed in the shape of the part cross section (Figure 2). Next, the platform supporting the powder bed lowers to allow for a new layer of powder. A heat lamp then radiates over the powder bed to partially cure the liquid binder. The hopper hovers over the powder bed and oscillates to deposit powder, which is

immediately flattened by a roller. The printhead deposits binder in the shape of the next cross section and the process repeats until the part is complete. The powder bed is then withdrawn from the machine and placed into an oven to fully cure the binder at 200 ℃ for 4 hours as recommended by the binder manufacturer. The green parts are now durable enough to be gently handled and are extracted from the powder bed. The parts can be subjected to post processing techniques, such as sintering or infiltrating with another material, where the binder evaporates and porosity is reduced.

2.2. Materials

The liquid binder used in these experiments is an ExOne standard proprietary aqueous solution (BA005) and possesses a density of 1.06 g/cm^3. The aluminum oxide powder, which has a purity of >99% and density of 3.95 g/cm^3, was manufactured via ball-milling and purchased from ExOne. The powder did not undergo any further treatment before use. A particle size analysis on powder images taken with a Scanning Electron Microscope (Quanta 600) show the powder has an average particle diameter of about 33 microns, D10 value of 20 microns, D90 value of 40 microns, and is highly prismatic in shape (Figure 3).

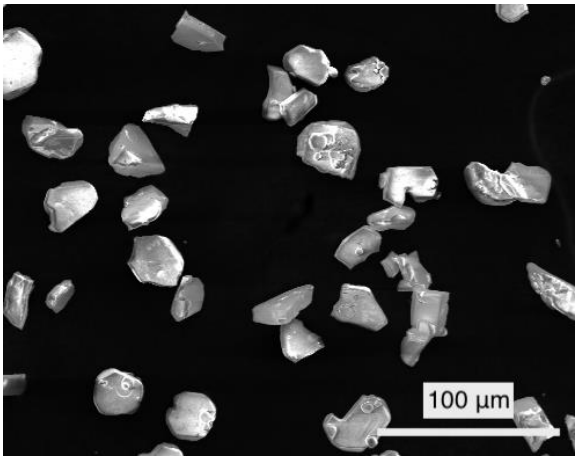

Figure 3. SEM Images of the highly prismatic alumina powder used in this study.

Table 1. Description of tested process inputs for ExOne Innovent binder jetting system

Parameter/Input	*Abbreviation*	*Description*
Layer Thickness (μm)	*La*	*distance the platform is lowered at the start of a new layer*
Recoat Speed (mm/s)	*Re*	*speed of hopper as it moves across the powder bed during powder deposition*
Oscillator Speed (rpm)	*Os*	*rate the powder hopper vibrates while it's depositing powder*
Roller Speed (mm/s)	*Ro*	*speed of roller as it flattens out the newly deposited powder*
Drying Time (sec)	*DT*	*duration the powder bed is exposed to the heat lamp*
Drying Power (%)	*DP*	*intensity of the heat lamp as it hovers over the powder bed*
Saturation Level (%)	*Sa*	*ratio of binder volume to volume of interstitial voids*

2.3. Parametric study

The quality of binder jetted parts can be significantly affected by changing printing parameters. In this study, the effects of seven operator-controlled process parameters (Table 1) were explored. A methodical approach should be used to plan a set of builds suitable for extracting information regarding the influence of the process input's on green densities. A full factorial design of experiments, which accounts for every possible process input combination, consisting of 3 settings/levels for each input can be used. However, that would result in 3_7 or 2187 builds; a poor use of time and materials. Instead, this study determines the effect of the seven inputs with the least amount of experiments possible using an orthogonal design, a type of partial factorial experimental design [31]. An L18 orthogonal array outlines the input combinations for 18 experiments and accounts for eight process parameters, where one parameter will have two levels and the rest will have three levels. The levels of each parameter were determined experimentally by finding a range of values for each input that would produce adequate powder spreading, provide an amount of binder for acceptable layer adhesion, and allow the binder to partially cure. Since this experiment considers only seven process parameters, the eighth parameter, labeled "blank",

Table 2. L18 partial factorial array with specified process parameters for each experiment

Experiment	*Layer Thickness (μm)*	*Recoat Speed (mm/sec)*	*Oscillator Speed (rpm)*	*Roller Speed (mm/sec)*	*Drying Time (sec)*	*Drying Power (%)*	*Saturation Level (%)*	*Blank*
1	66	20	2500	20	25	25	50	A
2	66	20	3500	75	50	50	70	B
3	66	20	4500	130	75	75	90	C
4	66	50	2500	20	50	75	90	B
5	66	50	3500	75	75	25	50	C
6	66	50	4500	130	25	50	70	A
7	66	80	2500	75	75	50	90	A
8	66	80	3500	130	25	75	50	B
9	66	80	4500	20	50	25	70	C
10	100	20	2500	130	50	50	50	C
11	100	20	3500	20	75	75	70	A
12	100	20	4500	75	25	25	90	B
13	100	50	2500	75	25	75	70	C
14	100	50	3500	130	50	25	90	A
15	100	50	4500	20	75	50	50	B
16	100	80	2500	130	75	25	70	B
17	100	80	3500	20	25	50	90	C
18	100	80	4500	75	50	75	50	A

was not allocated a process input. The layer thickness parameter was given two levels to represent about two and three times the average particle size. Table 2 tabulates the process inputs for each of the 18 experiments.

2.4. Density characterization

Three prisms with dimensions of 15 x 20 x 25 mm were printed for each of the 18 experiments (Figure 4). The relative density of these green parts cannot be measured using the conventional Archimedes' method for additively manufactured parts (ASTM B962, 2008) [23] because the cured binder will dissolve upon being submerged in the fluid and compromise the integrity of the binder jetted green parts. As such, the green densities of these prisms were measured using the geometric density approach [32]. In this approach, the mass of the prism, measured using a Fisher Scientific SLF103 scale with a resolution of 0.001 g, is divided by its

volume, measured with a Vinca DCLA-0605 digital caliper that has a resolution of 0.01 mm. Measurements were replicated 5 times to ensure accuracy.

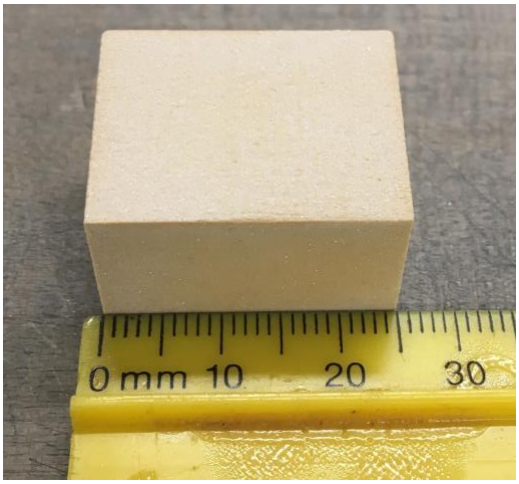

Figure 4. Binder jetted green prism

2.5. Statistical analysis

A main effect analysis is utilized to qualitatively compare the influence of each process input on the experimental response (i.e. printed densities). The effect of an input *A* at the level *i* ($E_{A(i)}$) on the response *Y* is computed using Equation (1)

$$E_{A(i)} = \bar{Y}_{A(i)} \tag{1}$$

where $\bar{Y}_{A(i)}$ is the average of all the responses when the input *A* is at the level *i*, regardless the value of other inputs. An input's main effect (F_A) is defined as the range of the input's effects at different levels:

$$F_A = \mathrm{Max}\left(E_{A(i)}\right) - Min\left(E_{A(i)}\right) \tag{2}$$

The main effect analysis assumes the process inputs are not interdependent, which is the case for the independent inputs in the binder jetting process. The larger the magnitude of the main effect, the more influence the process input has on the measured output.

Analysis of variance (ANOVA), an alternative statistical analysis, is widely utilized to study the influence of a process input by comparing its effect to that of experimental error [33]. This analysis consists of partitioning the total sum of squares into components related to the input effects and experiment error, as shown in Equation (3).

$$SS_{Total} = SS_{Factors} + SS_{Error} \tag{3}$$

The total variance is the sum of squares of all the measured data:

$$SS_{Total} = \sum\left(\rho_{jl} - \overline{\rho_{jl}}\right)^2 \quad (j = 1,2,\dots,18; l = 1,2,3) \tag{4}$$

where ρ is the experimental response, *j* is the test number, and *l* is the sample number. In this study, the total variance is divided as shown in Equation (5).

$$SS_{Total} = SS_{Re} + SS_{Os} + SS_{Ro} + SS_{La} + SS_{Sa} + SS_{DT} + SS_{DP} + SS_{Error} \tag{5}$$

A variance component pertaining to an input, such as roller speed (Re), is calculated using Equation (6), which is the sum of squares of the response (ρ) among different levels.

$$SS_{Re} = \sum_{l=1}^{3}\left(\overline{\rho_{Re=level\_\imath}} - \overline{\rho_{jl}}\right)^2 \tag{6}$$

The variance component pertaining to experimental error is the sum of squares of the response (ρ) at the same levels:

$$SS_{Error} = \sum_{l=1}^{3}\left(\rho_{jl}|_{Re=level\_i} - \overline{\rho_{Re=level\_\imath}}\right)^2 \tag{7}$$

The bias introduced by the number of samples on a calculated *SS* should be removed by dividing the *SS* components with the degrees of freedom (DOF), which is one less than the respective sample size. Mean squares (MS) are defined as

$$MS_{Re} = \frac{SS_{Re}}{DOF_{Re}} \tag{8}$$

A Fisher test (F-test) is applied to test the significance of an input by calculating the ratio between the input's MS and the experimental error's MS:

$$F_{Re} = \frac{MS_{Re}}{MS_{Error}} \tag{9}$$

Finally, p-values for each input can be extrapolated from a p-value table as a function of the input's F-value, the input's DOF, and the experimental error's DOF (Equation (10)). These P-values can be used to determine an input's "statistically significant". Minitab software calculated the p-values for each process input.

$$P_{Re} = f(F_{Re}, DOF_{Re}, DOF_{Error}) \tag{10}$$

A statistical model can be developed using a multivariable linear regression to predict printed densities as a function of the seven process inputs. Such a model can be written as

$$\rho_{relative} = b + \beta_1 Re + \beta_2 Os + \beta_3 Ro + \beta_4 La + \beta_5 Sa + \beta_6 DT + \beta_7 DP \tag{11}$$

where $\rho_{relative}$ is the relative density, b is the y-intercept, the beta coefficients are values that produce the best fitting via least squares, *Re* is the recoat speed, *Os* is the oscillator speed, *Ro* is the roller speed, *La* is the layer thickness, *Sa* is the saturation level, *DT* is the drying time, and *DP* is the drying power. The beta coefficients can be interpreted as the expected change in the output (i.e. green density) with respect to the change in input; the larger the magnitude, the larger the effect of the input on the output. As seen in Table 2, the process inputs are of various scales, so the value of beta coefficients are dependent on the scale of the values. Before subjecting the inputs to a linear regression analysis, they should be standardized to remove such bias using the following equation:

$$x = \frac{x_{nom} - x_{ave}}{x_{max} - x_{min}} \tag{12}$$

where x_{nom} is the input level being standardized, x_{ave} is the averaged value of that input range, x_{max} is the largest value for that input range, and x_{min} is the smallest value for that input range. A least-squares approach is utilized to determine the best-fitting beta coefficients for the data by minimizing the sum of squares of the residuals (the difference between the experimental and

predicted values) for all inputs. A preloaded function in R, a statistical programming language, performed the linear regression and calculated the beta coefficients to generate a linear model for predicting the printed densities [34].

Although a linear model can help characterize the key dependencies between output and input variables with small datasets, using it to identify optimal print conditions is limiting as the optima may occur at the boundary of the domain (min or max values of the input variables). To address this issue, a more complex Gaussian process regression method was also used that models the relative green density at a point $x = (Re, Os\ Ro, La, Sa, DT, DP)$ as a draw from Gaussian process with mean function $\mu(x)$ and covariance function $\sigma(x, x)$.

$$\rho_{relative}(x) \sim Gaussian(\mu(x), \sigma(x, x)) \tag{13}$$

The method starts with an initial guess for the expected relative green density (e.g. $\mu_0(x) = 0$) and covariance function which indicates how correlated the densities at input points *x*, *x'* are expected to be. Typically, $\sigma_0(x, x')$ is chosen to be one of the standard kernel functions in machine learning; since the result did not change when the length-scale parameter was varied from 0.1 to 15, we used the Matern kernel with length scale 15. After observing data, the expected green density function and covariance function are updated as

$$\mu(x) = x^T(\sigma_0(X, X))^{-1}Y \tag{14}$$

$$\sigma(x, x') = \sigma_0(x, x') - \sigma(x, X)(\sigma(X, X))^{-1}\sigma(X, x) \tag{15}$$

where $X = [x_1, \dots, x_n]$ is the set of input settings in the data and $Y = [y_1, \dots, y_n]$ are the corresponding green densities observed. If a linear kernel $\sigma(x, x') = x^T x'$ is used, Equation (14) is the same update as a linear regression fit. An illustration of the method is shown in Figure 5. The Gaussian process regression model allows for modeling complex non-linear relations and

quantifies associated uncertainties. The optimum process parameter settings for input variables are then chosen as the ones that maximize the upper confidence bound $\mu(x) \pm 10\sqrt{\sigma(x,x)}$.

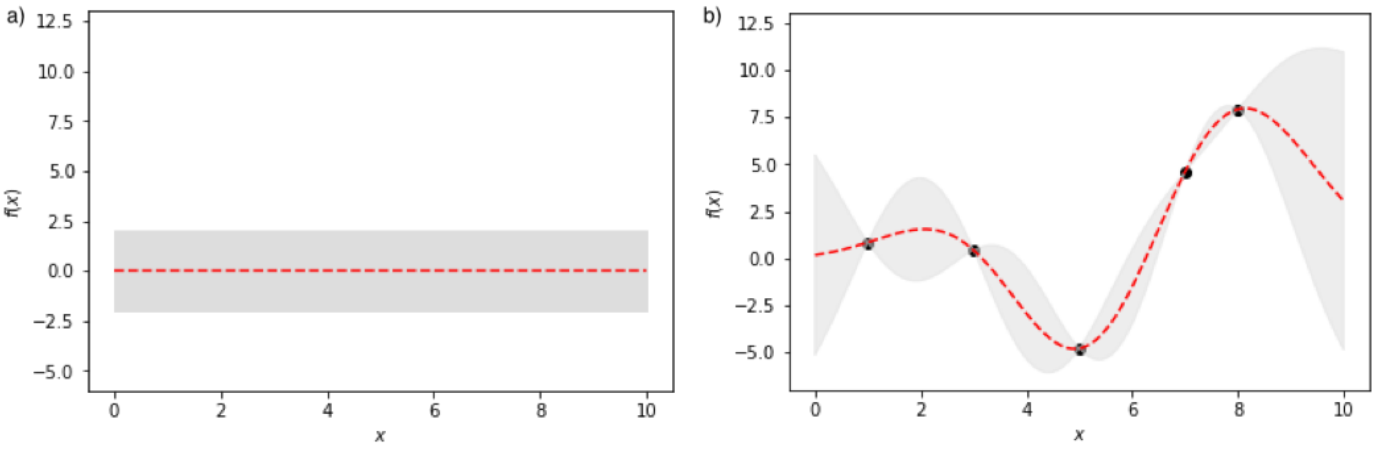

Figure 5. (a) Prior mean function $\boldsymbol{\mu_0(x)}$ as red dashed line and confidence band ($\boldsymbol{\mu_0(x) \pm 2\sqrt{\sigma_0(x,x)}}$). (b) Posterior mean function $\boldsymbol{\mu(x)}$ as red dashed line and confidence band ($\boldsymbol{\mu(x) \pm 2\sqrt{\sigma(x,x)}}$) after fitting to data.

3. RESULTS AND DISCUSSION

3.1. Density

All 18 batches were printed successfully (Figure 6a). Green densities were measured and converted to relative densities or packing efficiencies using the following equation:

$$\rho_{relative} = \frac{\rho_{green}}{\rho_{bulk}} * 100\% \quad (16)$$

where $\rho_{relative}$ is the relative density or packing efficiency, ρ_{green} is the measured green density, and ρ_{bulk} is the theoretical density for bulk α phase alumina (3.95 g/cm^3). Average relative densities and the ranges for each experiment are shown in Figure 6b, where the x-axis is the experiment number and y-axis is the respective relative density.

Despite working with similar particle sizes, the relative densities (30-45%) of the eighteen experiments in this study are noticeably lower than those reported in other binder jetting studies (45-65%) [9] [31] [32] [39] [40]. The large discrepancy in green densities can be attributed to the

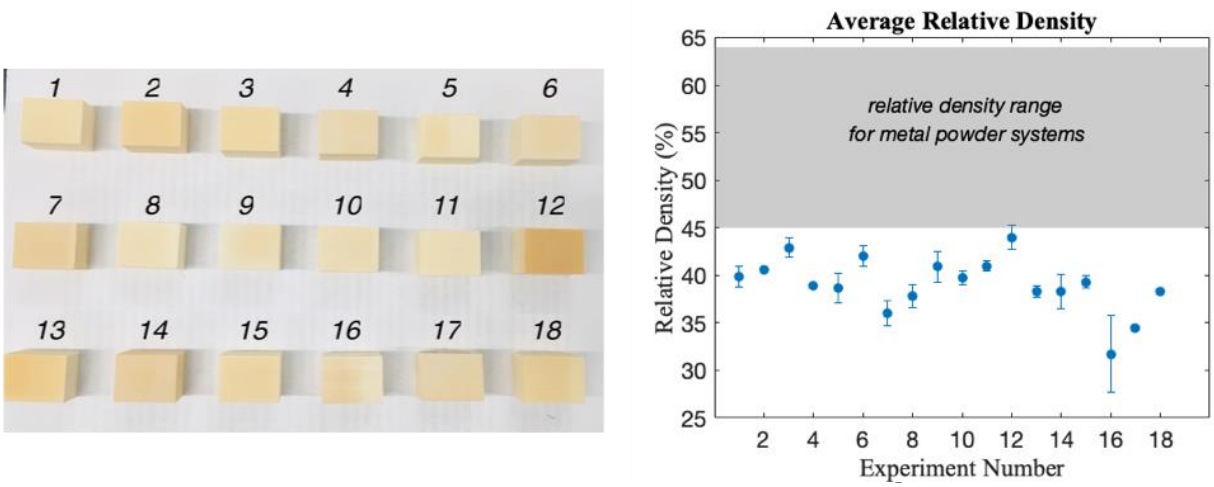

Figure 6. (a) One prism from each of the 18 builds. (b) The average relative density of each build is within a 30-45% range, lower than that of binder jetted metal samples (45-65%) reported in [9] [31] [32] [39] [40].

differences in packing efficiencies and flowability of the powder systems. Metal binder jetting processes typically utilize gas-atomized metal powder [37], spherical in nature, while the experiments in this study utilized ball-milled alumina powder, highly prismatic in nature. Particle shape (Figure 3) heavily influences packing efficiencies, where deviations from a spherical shape decrease packing efficiencies due to the increase in probability of forming bridges between particle corners and an increase in interparticle friction [38]. Therefore, ball-milled ceramic powder systems are expected to have lower packing efficiencies than gas-atomized metal powder systems. Other additive manufacturing studies also observed similar differences in packing behavior between spherical and prismatic powders [39].

Despite the relatively low printed densities, the powder system can be modified to increase the packing efficiencies in the powder bed. Bai et al. demonstrated printed and sintered densities of binder jetted parts can be increased by mixing two powder systems to form a bimodal size distribution [27]. Packing efficiencies can also be increase by substituting the prismatic, ball-milled ceramic powder with spherical ceramic powder; albeit, such powder is typically manufactured using more expensive and lower yielding processes like sol-gel synthesis [40].

Table 3. The main effect calculations of the seven process inputs. Average relative densities for all levels of each process input are shown. Main effect the range of these averages for each process input. The influence of each input on relative density is ranked based on the magnitude of their main effect, a greater main effect signifies a larger influence.

Level	Layer thickness (μm)	Recoat speed (mm/s)	Oscillator speed (rpm)	Roller traverse speed (mm/s)	Drying time (s)	Drying power (%)	Saturation level (%)	Blank
Level 1	39.74	41.35	37.42	39.07	39.40	38.92	38.95	39.25
Level 2	38.33	39.25	38.47	39.32	39.45	38.67	39.08	38.72
Level 3	-	36.52	41.23	38.73	38.27	39.53	39.08	39.15
Main Effect	1.41	4.83	3.82	0.58	1.18	0.87	0.13	0.53
Rank	③	①	②	⑥	④	⑤	⑧	⑦

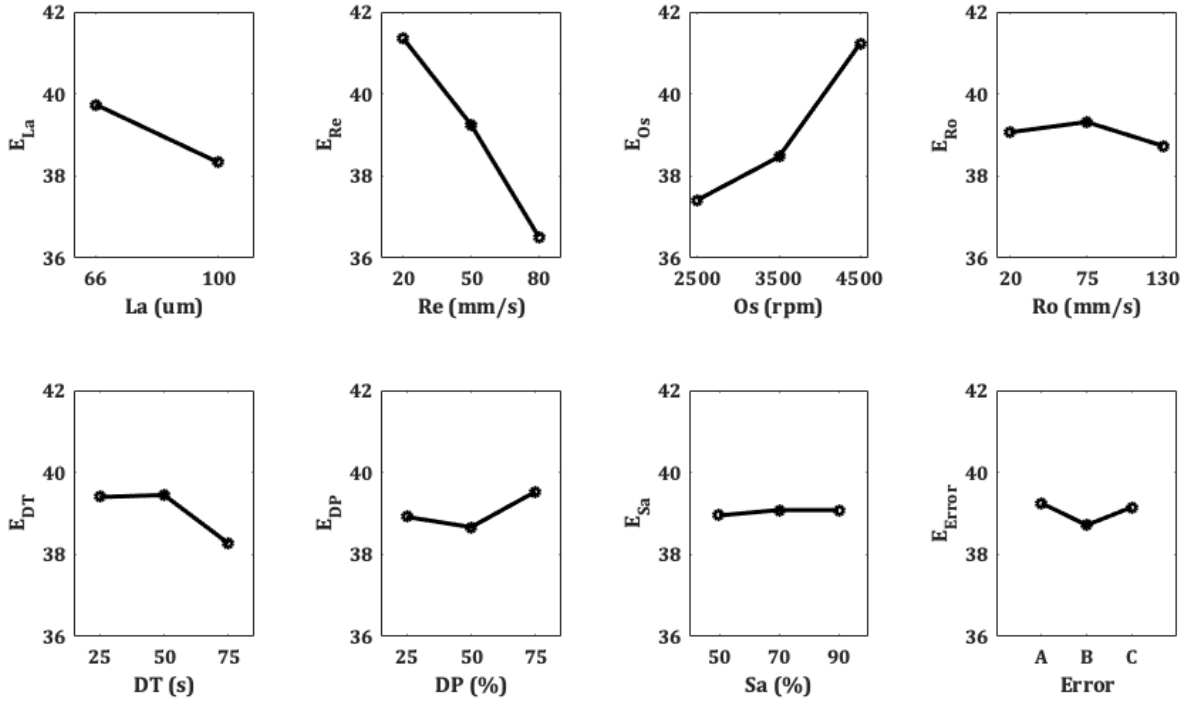

Figure 7. The effect of the seven studied process inputs on the relative density of binder jetted samples. Each point represents the average relative density at that process input level. The "Blank" column captures the effect of random and experimental errors.

3.2. Main effect and analysis of variance for process inputs

Main effects can be visually examined by plotting the average densities for every level of a single process input, as seen in Figure 7. A larger difference between the maximum and minimum values implies a larger influence by that input. Table 3 shows the average measured densities for each level and main effect for each input. The influence of the process inputs on relative densities can be ranked by ordering the magnitude of the main effect of the process inputs. Such ranking yields: ***Recoat Speed > Oscillator Speed > Layer Thickness> Drying Time > Drying Power > Roller Speed > Blank > Saturation Level.*** The main effect of the "blank" column, which hosts no input, represents the influence of random and experimental error on the printed density. Process inputs with a smaller main effect than the blank column may be considered to have a negligible effect on the printed density. With that said, a more thorough approach should be taken to more accurately define which inputs have significant effects.

ANOVA provides a sophisticated means for determining whether a process input possesses a significant or insignificant effect on the printed densities. Minitab software performed an ANOVA to calculate the p-values for every process input. Table 4 shows the p-value, degrees of freedom (DoF), sum of squares (SS), mean square (MS) and F-value for each process input.

Table 4. ANOVA for the process inputs and blank column. A P-value is calculated as a function of the degrees of freedom, specified inputs, and measured outputs. P-values lower than 0.05 are considered to have a noticeable effect on the process output (i.e. relative density).

Source	DoF	SS	MS	F-value	P-value
Layer thickness (μm)	1	27.4	27.4	9.6	0.004
Recoat speed (mm/sec)	2	211.4	105.7	36.9	0.000
Oscillator speed (rpm)	2	139.8	69.9	24.4	0.000
Roller traverse speed (mm/s)	2	3.3	1.7	0.6	0.564
Drying time (sec)	2	16.0	8.0	2.8	0.073
Drying power (%)	2	6.8	3.4	1.2	0.315
Saturation level (%)	2	0.3	0.1	0.1	0.954
Blank	2	2.9	1.4	0.5	0.617
Total error	38	111.6	2.9		
Sum	53	519.4			

Generally, a p-value of 0.05 is chosen as the threshold to determine if a process input significantly affects the process outcome [31]. Based on this criteria, three process inputs significantly affect the printed density (P-value < 0.05): recoat speed, oscillator speed, and layer thickness.

Recoat speed and oscillator speed directly control the amount of powder deposited onto the powder bed, suggesting depositing more powder increases the powder bed density because a higher quantity of powder will increase the likelihood of small particles settling within the interstitials of the larger particles. Increasing the oscillation speed further agitates the powder in the hopper; this increases the tapping effect in the hopper which causes the finer particles with higher packing efficiencies to be deposited onto the powder bed before the larger particles. Reduction in layer thickness decreases the volume the newly deposited powder needs to occupy, which increases the probability of the interstitials being occupied by finer particles. Saturation level has no significant effect in the final densities since most of the binder is evaporated during the curing process, and it is estimated that the weight percentage of the binder is less than 1% of the entire green part [41]. An SEM image (Figure 8) of a binder jetted green part shows minimal traces of binder. The roller appears to not pick up the deposited powder so the speed at which it moves across the powder has no effect on the powder packing efficiency. Drying time and drying

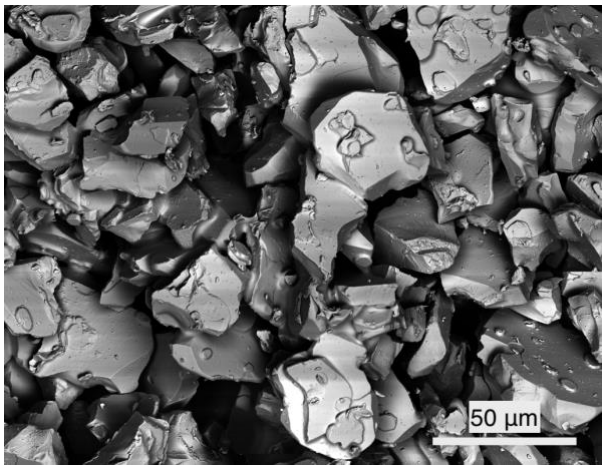

Figure 8. Powder particles bound together within a binder jetted green part show little traces of binder.

power control the partial evaporation of the binder during the build process. The two inputs affect the amount of binder in the green parts and have a minor influence on the weight of the green parts.

3.3. Linear regression model and process mapping

The normalized process inputs for the 18 experiments and respective measured densities were fed into a linear regression function, resulting in a y-intercept of 39.025 and coefficients shown in Table 5. Consolidating the calculated coefficients into a linear equation yields:

$$\rho_{relative} = 39.025 - 4.831(Re) + 3.821(Os) - 0.347(Ro) - 1.423(La) + 0.152(Sa) + 1.119(DT) + 0.601(DP) \quad (13)$$

The magnitude of the beta coefficients can be directly compared, because the process inputs were normalized using Equation (12) prior to performing the regression analysis. Ranking coefficient magnitudes indicates recoat speed and oscillator speed are the most influential parameters with layer thickness and drying time having minor influences. This is in agreement with the main effect and ANOVA analyses.

Using the linear model in Equation (13), the expected relative densities can be plotted in a process map as a function of the oscillator speed and recoat speed (Figure 9). The process map shows diagonal bands, from the bottom left corner to the top right corner, of equal relative densities. The average experimental measurements are plotted as black markers. According to the linear

Table 5. Beta coefficients calculated from linear regression

Parameter Input	$Regression\ Coefficients$ β_i
Layer thickness (μm)	-1.423
Recoat speed (mm/sec)	-4.831
Oscillator speed (rpm)	3.821
Roller traverse speed (mm/s)	-0.347
Drying time (sec)	1.119
Drying power (%)	0.601
Saturation level (%)	0.152

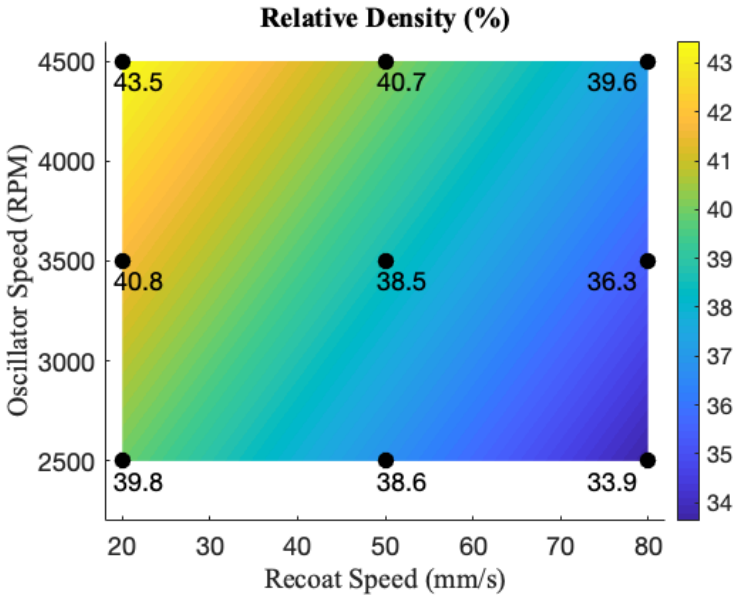

Figure 9. The expected green densities can be plotted as a function of recoat speed and oscillator speed using Equation 4. Overlapping the experimental measurements on the process space shows the linear model is a good fit. The process map suggests the green density of a binder jetted part can be increased by increasing oscillator speed and decreasing recoat speed.

model and process map, the layer thickness should be decreased, and the oscillator speed-recoat speed combination should occupy the top-left space (highest oscillator and lowest recoat speed) to maximize green densities.

One print was conducted with process input combinations not included in the prior 18 prints to validate the accuracy of the linear model. The levels of the seven process inputs were chosen as: Re = 20 mm/s, Os = 4000 rpm, Ro = 75 mm/s, La = 66 μm, Sa = 70%, DT = 50 s, and DP = 50%. The linear model predicts the binder jetting process will print an alumina part with a relative density of 43.1% with the mentioned process inputs. Three prisms with the dimensions mentioned in Section 2.4 were printed. The relative densities of these green parts were 43.4%, 42.2%, and 41.6% (average of 42.4%). The good agreement between the experimental and predicted density proves a linear model can help in deciding which process inputs should be selected for a desired outcome.

Another print was conducted in an attempt to maximize the density of the green samples by increasing the oscillation speed and decreasing the recoat speed to process parameters outside the process region tested in the parametric study. The levels of the seven process inputs were chosen as: *Re* = 10 mm/s, *Os* = 4800 rpm, *Ro* = 94.2 mm/s, *La* = 66 μm, *Sa* = 50%, *DT* = 41.6 s, and *DP* = 60.7%. The linear model predicts a printed density of 45.3% using these printing parameters. Twelve prisms with the dimensions described in Section 2.4 were printed, and their average density was 46.8% with a standard deviation of 1.9%. Although the expected model was within one standard deviation of the measured average, it proved to be less accurate for this print than the previous one. This was expected since the process parameters were outside the processing space from which the model was generated. As such, one should incorporate results from process parameters outside the processing space to expand the boundaries of the model before calculating the expected densities at these parameters.

3.4. Gaussian process regression model and optimal print density

Using a linear model to identify optimal print conditions is limiting as the optima only occur at the boundary of the domain (min or max values of the input variables). To address this, a Gaussian process regression model as described in Section 2.5 was also fitted to the data from the 18 experiments. The accuracy of this model for the validation print corresponding to setting *Re* = 20 mm/s, *Os* = 4000 rpm, *Ro* = 75 mm/s, *La* = 66 μm, *Sa* = 70%, *DT* = 50 s, and *DP* = 50% was 41.6% which is close to the average experimental density of 42.4%. The optimal print conditions suggested by the Gaussian process model for the 7 process inputs were: *Re* = 20 mm/s, *Os* = 4800 rpm, *Ro* = 94 mm/s, *La* = 92 μm, *Sa* = 80%, *DT* = 42 s, and *DP* = 61%. Note that the process settings suggested by Gaussian process model agree with the linear model for the two most

significant process parameters (*Re* and *Os*). However, the Gaussian process model suggests a non-linear trend with remaining parameters, and the optimal setting is not achieved at the max/min value for these parameters. Twelve prisms with geometry specified in Section 2.4 were printed with this optimal parameter combination. The average relative density of the prisms was 47.3% with standard deviation of 2.7% and range of 7.4%. The variability is due to the inhomogeneous powder packing within the powder bed. It can be seen that the optimal parameters produce samples with relative densities in the bounds of metal powder systems (45-65%) just by tuning process parameters.

4. CONCLUSIONS

A linear regression sensitivity analysis has determined that out of 7 process parameters, recoat speed and oscillator speed have the greatest influence on printed densities (green densities) of binder jetted alumina. Layer thickness and drying time have secondary influences, and the other three parameters, roller transverse speed, drying power and saturation level had minimal influences. As a result, green density can effectively be approximated as a function of recoat speed and oscillator speed in a 2-parameter fit. A linear regression and Gaussian process regression gave similar results when predicting green densities. This is due to nonlinearity of process variable dependence primarily being exhibited in the five process variables other than recoat speed and oscillator speed. Both of the parameter fitting methods allow for effective extrapolation and indicate the optimal alumina part density is near 47%, which is at the low end of densities seen in binder jet printing of spherical metal powders. Although not rigorously tested in this work, it is also expected that each of the parameter fitting methods would be effective at interpolation to purposefully manipulate green density. Optimal green density is near the tap density for the

alumina powder, suggesting tap density as the upper bound for any parametric study optimizing green density. Surface tension effects of introducing the binder do not appear to affect density. This is consistent with micrographs of binder jetted alumina after drying that show very little binder between particles. The relatively low density for binder jetted alumina powder appears to be due primarily to the irregular particle morphology. Thus, further increases in binder jetted density can be achieved by altering the powder morphology and/or particle size distribution to allow for better particle packing.

5. ACKNOWLEDGEMENTS

Edgar Mendoza Jimenez acknowledges support from the National Science Foundation (NSF) Graduate Research Fellowship (award number DGE1745016). B. Reeja-Jayan acknowledges support from her NSF Career (award number CMMI1751605). Support from CMU NextManufacturing Center and Manufacturing Futures Institute (MFI) is also acknowledged. Machine learning efforts were supported by the DARPA AIRA Program (grant number HR00111990030). The authors acknowledge Todd Baer at Carnegie Mellon University's NextManufacturing Center for assistance in handling binder jetting equipment and Carnegie Mellon University's Materials Science & Engineering department for access to the Quanta600 Scanning Electron Microscope (SEM).

6. REFERENCES

[1] W.E. Frazier, Metal additive manufacturing: A review, J. Mater. Eng. Perform. 23 (2014) 1917–1928. doi:10.1007/s11665-014-0958-z.

[2] M. Seifi, A. Salem, J. Beuth, O. Harrysson, J.J. Lewandowski, Overview of Materials

Qualification Needs for Metal Additive Manufacturing, Jom. 68 (2016) 747–764. doi:10.1007/s11837-015-1810-0.

[3] A. Badev, Y. Abouliatim, T. Chartier, L. Lecamp, P. Lebaudy, C. Chaput, C. Delage, Photopolymerization kinetics of a polyether acrylate in the presence of ceramic fillers used in stereolithography, J. Photochem. Photobiol. A Chem. 222 (2011) 117–122. doi:10.1016/j.jphotochem.2011.05.010.

[4] V.K. Balla, S. Bose, A. Bandyopadhyay, Processing of bulk alumina ceramics using laser engineered net shaping, Int. J. Appl. Ceram. Technol. 5 (2008) 234–242. doi:10.1111/j.1744-7402.2008.02202.x.

[5] Z. Fan, M. Lu, H. Huang, Selective laser melting of alumina: A single track study, Ceram. Int. 44 (2018) 9484–9493. doi:10.1016/j.ceramint.2018.02.166.

[6] J.A. Gonzalez, J. Mireles, Y. Lin, R.B. Wicker, Characterization of ceramic components fabricated using binder jetting additive manufacturing technology, Ceram. Int. 42 (2016) 10559–10564. doi:10.1016/j.ceramint.2016.03.079.

[7] J. Deckers, J. Vleugels, J.P. Kruth, Additive manufacturing of ceramics: A review, J. Ceram. Sci. Technol. 5 (2014) 245–260. doi:10.4416/JCST2014-00032.

[8] E. Sachs, J. Haggerty, M. Cima, W. Paul, Three-Dimensional Printing Techniques, 1993.

[9] Y. Bai, C.B. Williams, An Exploration of Binder Jetting of Copper, (n.d.) 793–814.

[10] H. Chen, Y.F. Zhao, Process parameters optimization for improving surface quality and manufacturing accuracy of binder jetting additive manufacturing process, Rapid Prototyp. J. 22 (2016) 527–538. doi:10.1108/RPJ-11-2014-0149.

[11] S.M. Gaytan, M.A. Cadena, H. Karim, D. Delfin, Y. Lin, D. Espalin, E. MacDonald, R.B. Wicker, Fabrication of barium titanate by binder jetting additive manufacturing

technology, Ceram. Int. 41 (2015) 6610–6619. doi:10.1016/j.ceramint.2015.01.108.

[12] L. Rabinskiy, A. Ripetsky, S. Sitnikov, Y. Solyaev, R. Kahramanov, Fabricati on of porous silicon nitride ceramics using binder jetting technology, IOP Conf. Ser. Mater. Sci. Eng. 140 (2016). doi:10.1088/1757-899X/140/1/012023.

[13] The Freedonia Group Inc, Industry Study #2794, Advanced Ceramics, 2011.

[14] K. Rajab, M. Naftaly, E. Linfield, J. Nino, D. Arenas, D. Tanner, R. Mittra, M. Lanagan, Broadband dielectric characterization of aluminum oxide (Al2O3), J. Microelectron. Electron. Packag. 5 (2008) 101–106. doi:10.4071/1551-4897-5.1.1.

[15] M.N. Afsar, Precision Millimeter-Wave Dielectric Measurements of Birefringent Crystalline Sapphire and Ceramic Alumina, IEEE Trans. Instrum. Meas. IM–36 (1987) 554–559. doi:10.1109/TIM.1987.6312739.

[16] E. Medvedovski, Ballistic performance of armour ceramics: Influence of design and structure. Part 1, Ceram. Int. 36 (2010) 2103–2115. doi:10.1016/j.ceramint.2010.05.021.

[17] S. Ghorai, K.K. Pant, Equilibrium, kinetics and breakthrough studies for adsorption of fluoride on activated alumina, Sep. Purif. Technol. 42 (2005) 265–271. doi:10.1016/j.seppur.2004.09.001.

[18] W. William J., Alumina Insulators for High Voltage Automotive Ignition Systems, in: Process. Prop. Des. Adv. Ceram. Compos. Ceram. Trans., 2016: pp. 361–370.

[19] L. Sedel, Evolution of Alumina-on-Alumina Implants, (2000) 48–54.

[20] N. Meethong, J. Sirirot, S. Srilomsak, Statistical Analysis of Composition and Temperature for Alumina Crucible Fabrication, 20 (2013) 317–327.

[21] M. MUNRO, Evaluated Material Properties for a Sintered alpha-Alumina, J. Am. Ceram. Soc. 80 (2005) 1919–1928. doi:10.1111/j.1151-2916.1997.tb03074.x.

[22] B. Amor, Ceramic Cutting Tools, 2018.

[23] H. Miyanaji, M. Orth, J.M. Akbar, L. Yang, Process development for green part printing using binder jetting additive manufacturing, Front. Mech. Eng. (2018) 1–9. doi:10.1007/s11465-018-0508-8.

[24] M. Doyle, K. Agarwal, W. Sealy, K. Schull, Effect of Layer Thickness and Orientation on Mechanical Behavior of Binder Jet Stainless Steel 420 + Bronze Parts, Procedia Manuf. 1 (2015) 251–262. doi:10.1016/j.promfg.2015.09.016.

[25] S. Shrestha, G. Manogharan, Optimization of Binder Jetting Using Taguchi Method, Jom. 69 (2017) 491–497. doi:10.1007/s11837-016-2231-4.

[26] A.M.M. Elliott, P. Nandwana, D. Siddel, B.G. Compton, A Method for Measuring Powder Bed Density in Binder Jet Additive Manufacturing Process and the Powder Feedstock Characteristics Influencing the Powder Bed Density, Solid Free. Fabr. 2016. Proceeding (2016) 1031–1037.

[27] Y. Bai, G. Wagner, C.B. Williams, Effect of Particle Size Distribution on Powder Packing and Sintering in Binder Jetting Additive Manufacturing of Metals, J. Manuf. Sci. Eng. 139 (2017) 081019. doi:10.1115/1.4036640.

[28] Y. Bai, C.B. Williams, No Title, (n.d.) 793–814.

[29] K.W. Desmond, E.R. Weeks, Influence of particle size distribution on random close packing of spheres, Phys. Rev. E - Stat. Nonlinear, Soft Matter Phys. 90 (2014) 1–6. doi:10.1103/PhysRevE.90.022204.

[30] S. Haeri, Y. Wang, O. Ghita, J. Sun, Discrete element simulation and experimental study of powder spreading process in additive manufacturing, Powder Technol. 306 (2017) 45–54. doi:10.1016/j.powtec.2016.11.002.

[31] S. Schmidt, Understanding Industrial Designed Experiments, 1992.

[32] A. Kantzas, B. Jonathan, S. Taheeri, Fundamentals of Fluid Flow in Porous Media, 2003.

[33] L. Su, J. Zhang, C. Wang, Y. Zhang, Z. Li, Y. Song, T. Jin, Z. Ma, Identifying main factors of capacity fading in lithium ion cells using orthogonal design of experiments, Appl. Energy. 163 (2016) 201–210. doi:10.1016/j.apenergy.2015.11.014.

[34] N. Matloff, The Art of R Programming, 2011.

[35] Y. Bai, G. Wagner, C.B. Williams, Effect of Bimodal Powder Mixture on Powder Packing Density and Sintered Density in Binder Jetting of Metals, 2015 Annu. Int. Solid Free. Fabr. Symp. (2015) 62. doi:10.1017/CBO9781107415324.004.

[36] H. Miyanaji, N. Momenzadeh, L. Yang, Effect of powder characteristics on parts fabricated via binder jetting process, Rapid Prototyp. J. (2018). doi:10.1108/RPJ-03-2018-0069.

[37] S. Kenzari, D. Bonina, J. Dubois, V. Fournée, Characterization of Metal Powders Used for Additive Manufacturing, 119 (2012) 460–493.

[38] A.B. Yu, N. Standish, Characterisation of non-spherical particles from their packing behaviour, Powder Technol. 74 (1993) 205–213. doi:10.1016/0032-5910(93)85029-9.

[39] C. Meier, R. Weissbach, J. Weinberg, W.A. Wall, A.J. Hart, Critical influences of particle size and adhesion on the powder layer uniformity in metal additive manufacturing, J. Mater. Process. Technol. 266 (2019) 484–501. doi:10.1016/j.jmatprotec.2018.10.037.

[40] M. Chatterjee, M.K. Naskar, B. Siladitya, D. Ganguli, Role of organic solvents and surface-active agents in the sol-emulsion-gel synthesis of spherical alumina powders, J. Mater. Res. 15 (2000) 176–185. doi:10.1557/JMR.2000.0029.

[41] T. Do, P. Kwon, C. Seop, Process development toward full-density stainless steel parts

with binder jetting printing, Int. J. Mach. Tools Manuf. 121 (2017) 50–60. doi:10.1016/j.ijmachtools.2017.04.006.